ACS APPLIED MATERIALS & INTERFACES

www.acsami.org

Research Article

Constructing a Multifunctional Interface between Membrane and Porous Transport Layer for Water Electrolyzers

Chang Liu, Klaus Wippermann, Marcin Rasinski, Yanpeng Suo, Meital Shviro, Marcelo Carmo,* and Werner Lehnert

Cite This: *ACS Appl. Mater. Interfaces* 2021, 13, 16182–16196

Read Online

ACCESS | Metrics & More | Article Recommendations | Supporting Information

ABSTRACT: The cell performance and durability of polymer electrolyte membrane (PEM) water electrolyzers are limited by the surface passivation of titanium-based porous transport layers (PTLs). In order to ensure stable performance profiles over time, large amounts ($\geq$1 mg·cm^{-2}) of noble metals (Au, Pt, Ir) are most widely used to coat titanium-based PTLs. However, their high cost is still a major obstacle toward commercialization and widespread application. In this paper, we assess different loadings of iridium, ranging from 0.005 to 0.05 mg·cm^{-2} in titanium PTLs, that consequently affect the investment costs of PEM water electrolyzers. Concerning a reduction in the precious metal costs, we found that Ir as a protective layer with a loading of 0.025 mg·cm^{-2} on the PTLs would be sufficient to achieve the same cell performance as PTLs with a higher Ir loading. This Ir loading is a 40-fold reduction over the Au or Pt loading typically used for protective layers in current commercial PEM water electrolyzers. We show that the Ir protective layer here not only decreases the Ohmic resistance significantly, which is the largest part of the gain in performance, but moreover, the oxygen evolution reaction activity of the iridium layer makes it promising as a cost-effective catalyst layer. Our work also confirms that the proper construction of a multifunctional interface between a membrane and a PTL indeed plays a crucial role in guaranteeing the superior performance and efficiency of electrochemical devices.

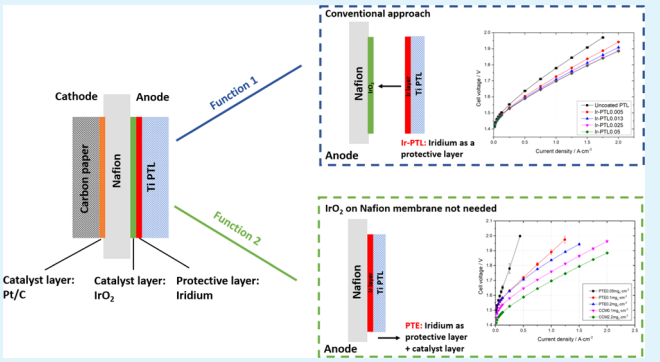

KEYWORDS: *PEM water electrolyzers, porous transport layer, porous transport electrode, iridium, sputtering*

1. INTRODUCTION

Electrolysis-generated hydrogen is the most promising energy carrier as it possesses high specific energy and is considered an environmentally friendly fuel.[1,2] Currently, hydrogen is mostly produced from fossil-based sources and therefore incurs a carbon signature during its production process.[3,4] However, water electrolysis coupled with renewable energy sources such as solar and wind is regarded as the technology of choice for sustainable energy conversion and posterior short- and long-term storage.[5,6] Among other types, a polymer electrolyte membrane (PEM) water electrolyzer primarily consists of a catalyst-coated membrane (CCM) sandwiched between two porous transport layers (PTLs) and bipolar plates. The PTL situated on the anode side is subjected to harsh oxidizing conditions as a result of the high cell overpotential, low pH, and oxygen gas evolution. Such conditions demand the use of highly corrosion-resistant PTLs and bipolar plates on the anode side. To circumvent this, PEM water electrolyzer components are typically made of titanium due to its excellent chemical stability, good conductivity, and high corrosion resistivity.[7,8] A variety of titanium-based PTL architectures including titanium felt,[9−12] mesh,[13,14] foam,[14,15] as well as sintered titanium powders[16−18] can be used in PEM electrolyzers. In recent decades, several research groups have investigated the effects of different parameters, such as thickness, particle size, pore diameter, and porosity in PTLs.[18−21] However, the passivation of titanium-based PTLs that occurs under real cell conditions is one of the essential factors that restricts their application in the absence of any surface modifications. Ti^0 changes its oxidation state over time due to the harsh anodic conditions, which leads to drastic degradation of PEM water electrolyzer cells.[22−24] For instance, in our previous studies, we observed a significant degradation rate of 194 μV·h^{-1} from a durability test over 1000 h and found that 78% of the degradation originated from titanium-based PTL degradation.[25]

Received: November 19, 2020
Accepted: March 8, 2021
Published: April 2, 2021

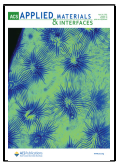

Table 1. Ir-Coated PTL Parameters and Corresponding Contact Resistance and Cell Voltage at 1 A·cm^{-2}

sample	sputter time/s	Ir loading/mg·cm^{-2}	contact resistance@3000 kPa/mΩ·cm^2	E@1 A·cm^{-2}/V
uncoated PTL	0	0	11.92	1.78
Ir-PTL0.005	30	0.005	5.50	1.73
Ir-PTL0.013	90	0.013	3.78	1.71
Ir-PTL0.025	180	0.025	3.06	1.70
Ir-PTL0.05	360	0.05	2.98	1.70

As a mitigation strategy, different methods of surface modification have already been reported in the literature. The titanium oxide layer of PTLs can be removed by means of etching. Compared to an untreated PTL, the TiH_x on the surface of a titanium PTL improved the electrical resistance and thus the cell's performance and durability.[24] Another more conventional and scalable approach is to use platinum group metal coatings as the protective layer on titanium-based PTLs. Noble metals such as platinum and gold are typically used to coat the titanium-based PTLs in PEM water electrolyzers.[25−27] A novel titanium PTL modified with an Au thin film achieved superior multifunctional performance and good short-term stability compared to conventional titanium PTLs.[26] In our previous study, platinum used as a protective coating exhibited a degradation rate of only 12 μV·h^{-1} and decreased Ohmic resistance, which confirmed that the Pt coating showed a positive effect on cell performance.[25] Nevertheless, the amounts of noble metal used as the protective layer in these studies were still very high, which significantly increased the cost of the PEM electrolyzers they focused on. Recently, we reported a scalable and simple method that entailed sputtering 20 nm-thick iridium layers to PTLs, which significantly decreased the contact resistance by 60 mΩ·cm^2 and the overpotential of the cells by 81 mV at 2 A·cm^{-2}. The total amount of iridium added was only 0.1 mg$_{Ir}$·cm^{-2}, which is around 10 times lower than the Au or Pt protective layers applied in other studies and current commercial electrolyzers.[9,28] More recently, we found that 4000 h of stable durability profiles are achieved when titanium-based PTLs are coated with only 0.1 mg·cm^{-2} of Pt or Ir. The results of this work show how the interface of a well-protected titanium fiber behaves against passivation after long-term operation under real electrolysis conditions.[29]

Iridium-based electrocatalysts are most commonly used in the anodes of PEM electrolyzers in terms of the oxygen evolution reaction (OER) due to their superior activity and durability; the use of the Ir layer on the PTL raised the question as to whether the Ir discussed here also features some activity that is beneficial to increasing the cell's performance. Few studies have shown the performance efficiency of thin catalyst layers on titanium-based PTLs for PEM water electrolyzers.[30,31] However, the thin layers on PTLs in these studies are for this study of less relevance as they were either applied on the cathode side of the electrolyzer or for high-temperature electrolysis applications.

Here, we show for the first time that the Ir coating on the PTL can be used not only as a protective layer to protect the titanium-based PTL from passivation but also to enhance the overall OER rate in order to gain additional cell performance. This offers a promising means to develop cost-effective PTLs for PEM water electrolyzers. Sputter-coated Ir thin films on titanium-based PTLs are not only proposed as a protective layer to protect titanium from passivation but also exhibit electrocatalytical properties, which makes them promising as cost-effective catalyst layers. From a broader perspective, the results of this work shed light on the importance of constructing a multifunctional interface between a membrane and a PTL in guaranteeing the superior performance of a water electrolyzer.

2. EXPERIMENTAL SECTION

2.1. Cleaning Procedure for the PTLs. The cleaning procedure for titanium-based PTLs was aimed at removing organic contaminants and substances. The PTLs were immersed in deionized water (Milli-Q) (18.2 MΩ cm) at 80 °C for 15 min. Then, they were immersed in 2-propanol and acetone in an ultrasonic bath at ambient temperature for 15 min. After that, they were rinsed twice in deionized water at 80 °C for 15 min and finally air-dried at ambient temperature overnight.[9]

2.2. Sputtering Step. The iridium layers were deposited on the PTLs by a plasma-sputtering instrument (Quorum Q150T). They were coated on each side with metallic iridium using a current of 30 mA and 0.7 Pa under Ar. The loading and thicknesses of the iridium layers were controlled by varying the sputtering time (30, 90, 180, 360, 720, and 1440 s, respectively). The loadings of iridium were calculated by weighing the PTL before and after sputtering, the results of which are shown in Table 1. The final Ir loading of the PTLs was calculated only for one side of them.

2.3. Manufacturing of CCMs. The CCM manufacturing process has been reported in our previous work.[9] The Nafion 117 membrane was used as the electrolyte. 60% Pt/C (HiSPEC 9100, Johnson & Matthey) and IrO_2 (Alfa Aesar, Premion, 99.99%) were used as the cathode and anode catalysts, respectively. To prepare the catalytic inks, the ionomer solutions (15% Nafion for the cathode and 10% for the anode) and catalyst powders were dispersed in mixtures of 2-butanol and water. The procedure was then followed by agitating the mixtures in an ultrasonic homogenizer for 5 min. The catalytic inks were then coated onto the inert decal substrates by an automated bar-coating device (CoatMaster 509 MCI, Erichsen GmbH & Co. KG, the dimension of the bar coating: L 610 mm, W 425 mm, H 210 mm). The electrode layers were dried at ambient temperature for 30 min. Finally, the dried electrode layers were hot-pressed on the Nafion 117 membrane at 130 °C, 16 MPa, and for 3 min. The final catalyst loading was ∼0.8 ± 3% mg$_{Pt}$·cm^{-2} Pt/C for the cathode and ∼2.2 ± 10% mg$_{Ir}$·cm^{-2} IrO_2 for the anode. The ratios of the ionomer and the catalyst were 1:4 for the cathode and 1:3 for the anode.

To investigate the OER activity of the Ir layer on the PTLs, the CCMs assembled using these Ir-coated PTLs were manufactured without IrO_2 on the anodic side but only with 0.8 mg$_{Pt}$·cm^{-2} on the cathodic side. The Ir-coated PTLs discussed here are referred to as porous transport electrodes (PTEs). The low loading CCMs, with only ∼0.1 mg·cm^{-2} IrO_2 at the anode and ∼0.8 mg·cm^{-2} Pt at the cathode, were used as a reference CCM when comparing the cell performance with the PTEs.

2.4. Single Cell Components and Assembly. Titanium felts from Bekaert, with a porosity of 68% and thickness of 350 μm, were used as the PTL at the anode of a PEM water electrolyzer cell. In all tests, Toray papers (TGP-H 120) with a thickness of 350 μm were used as the cathodic PTL. Pt-coated bipolar plates with pin-type flow fields were used in the anode. Nevertheless, the cathode's flow-field was also coated with gold in order to avoid the embrittlement of hydrogen. The cells were compressed using PEFE gaskets with a thickness of 0.3 mm at both the anode and the cathode at a torque of

https://doi.org/10.1021/acsami.0c20690
ACS Appl. Mater. Interfaces 2021, 13, 16182−16196

8 N m on each of the six bolts. The active area was 25 cm^2. The electrolyzer cell design used in this study is presented in Figure 1.

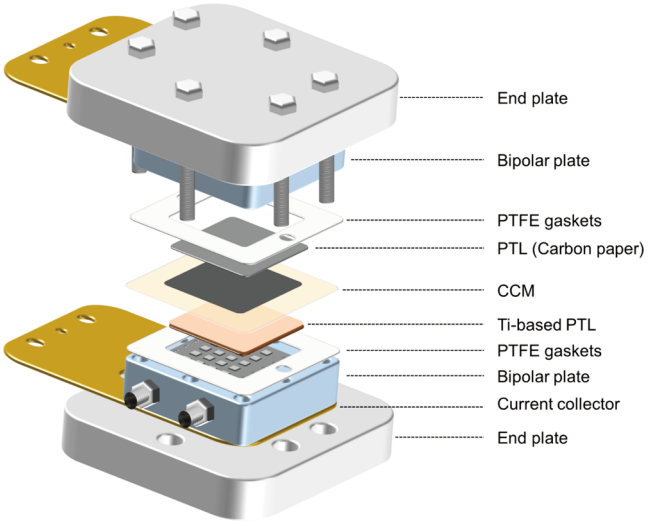

Figure 1. Schematic illustration of the 25 cm^2 PEM water electrolysis cell.

2.5. Electrochemical Measurements and Electrochemical Impedance Spectroscopy. All the single cell experiments were performed using E60 electrolyzer test benches from Greenlight. High-purity feed water (18.2 MΩ cm) was circulated through both the cathode and anode compartments in separate water circuits at flow rates of 50 mL min^{-1}. The temperature of the cell during operation was controlled by the flow of heated water supplied to the cell. Water and water/gas temperatures were sensed at the cell inlet and outlet. The temperature setpoint was defined as the cell inlet temperature. In addition, the cell was also heated by two heating cartridges which are inserted directly into the flow fields. Prior to the electrochemical cell tests, a break-in procedure was performed for each membrane electrode assembly (MEA). The single cell was heated up to 80 °C by applying temperature set points to the water flowing through both the cathode and the anode. A current density of 0.2 A·cm^{-2} was then applied to the cell for 30 min once the temperatures were reached. The current density was increased to 1.0 A·cm^{-2} for another 30 min thereafter. The single cell was operated at a constant voltage of 1.7 V until the current variation was less than 1% per hour. The measurement commenced from the open circuit. The current density was first increased in 0.0125 A·cm^{-2} steps to 0.25 A·cm^{-2} and then in 0.25 A·cm^{-2} steps until a limiting cell voltage of 2 V was achieved. The polarization curves were conducted in 5 min steps.

Electrochemical impedance spectroscopy (EIS) was conducted using a potentiostat (HCP 1005 from Biologic) following the polarization curve measurement at 80 °C. In the first section, regarding iridium on the PTL only working as a protective layer, EIS was conducted at a DC-bias of 0.15 A·cm^{-2} between 100 kHz and 100 mHz. The current perturbation was ±5% of the cell current, and the maximum voltage perturbation was 10 mV. In the second section, to investigate the OER activity for the Ir-coated PTLs (PTEs) in the second section, the EIS was conducted at DC-biases of 0.025, 0.05, 0.075, 0.1, 0.125, 0.25, 0.5, 0.75, 1.0, 1.25, 1.5, 1.75, and 2 A·cm^{-2} for all the CCM samples. It should be noted that the EIS spectra of the PTE samples were analyzed up to a maximum DC current density of only 0.25 A·cm^{-2} (PTE0.05) or 1 A·cm^{-2} (PTE0.1 and PTE0.2). This is because either the cell performance was very poor (PTE0.05) or the PTE samples spectra recorded at a DC current density >1 A·cm^{-2} were rather noisy and a simulation was not possible.

2.6. Physical and Chemical Characterizations. Scanning electron microscopy (SEM) (Zeiss Gemini Ultra Plus) was used to investigate the surface morphology of the PTLs. Energy-dispersive X-ray spectroscopy (EDX) was employed to investigate the chemical composition and mapping provided by the elemental distributions of the PTLs. A focused ion beam (FIB) (Zeiss Crossbeam 540 dual beam microscope) was applied to prepare the cross sections of the samples. On top of each PTL, two Pt coatings were deposited using an electron beam and ion beam, respectively. A double deposition process was conducted in order to protect the sample surface and the prepared cross section from the scattered ions, thus reducing the artifacts of the FIB milling (the so-called "curtaining effect").[32]

Contact resistance measurements were performed on all the PTLs at 25 °C. The samples were sandwiched between two Au-coated plates at a defined compression and probed for their through-plane resistance with a four-wire resistance measurement. The applied contact pressure was then varied from 800 to 6000 kPa by an electric press. The sum of the PTL resistance and two contact resistances between the PTL and Au-coated plates was determined using the

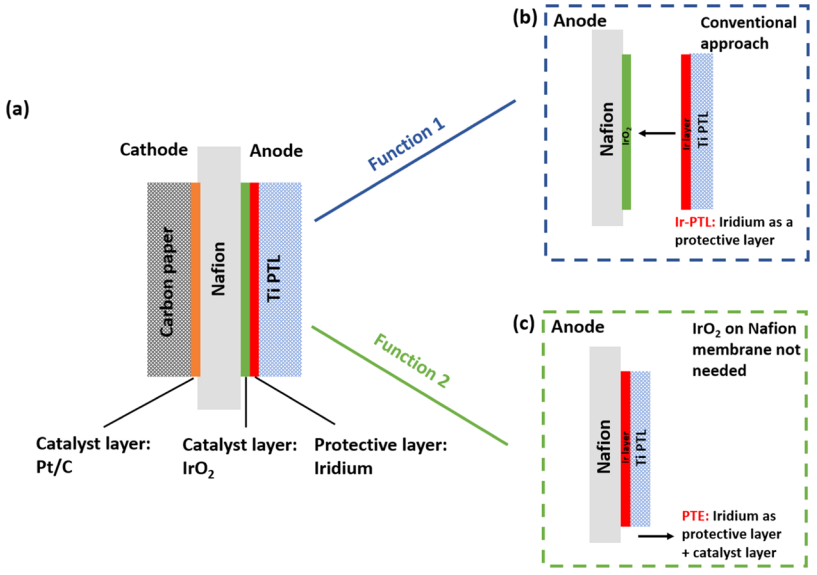

Figure 2. (a) Schematic illustration of the key components inside a PEM electrolyzer; (b) Ir-coated PTL assembled with a standard CCM, with the Ir layer on the PTL serving as a protective layer here (Ir-PTL); (c) Ir-coated PTL assembled with a CCM without IrO_2 on the membrane: the Ir layer served as a catalyst layer (PTE).

https://doi.org/10.1021/acsami.0c20690
ACS Appl. Mater. Interfaces 2021, 13, 16182−16196

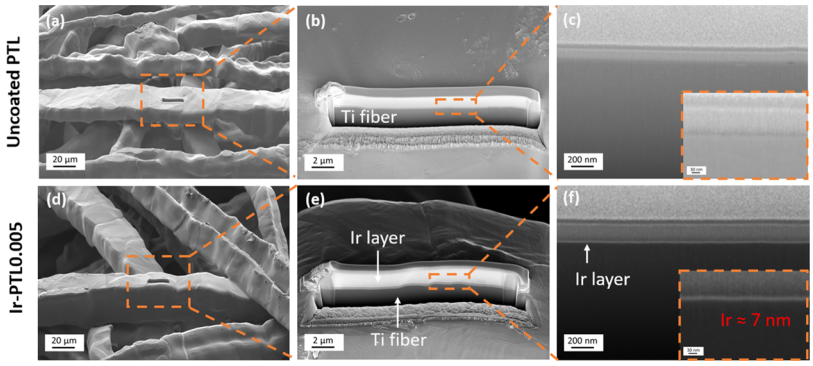

Figure 3. SEM images of FIB-prepared cross-sectional images of (a–c) an uncoated PTL and (d–f) an Ir-coated PTL0.005mg·cm^{-2}.

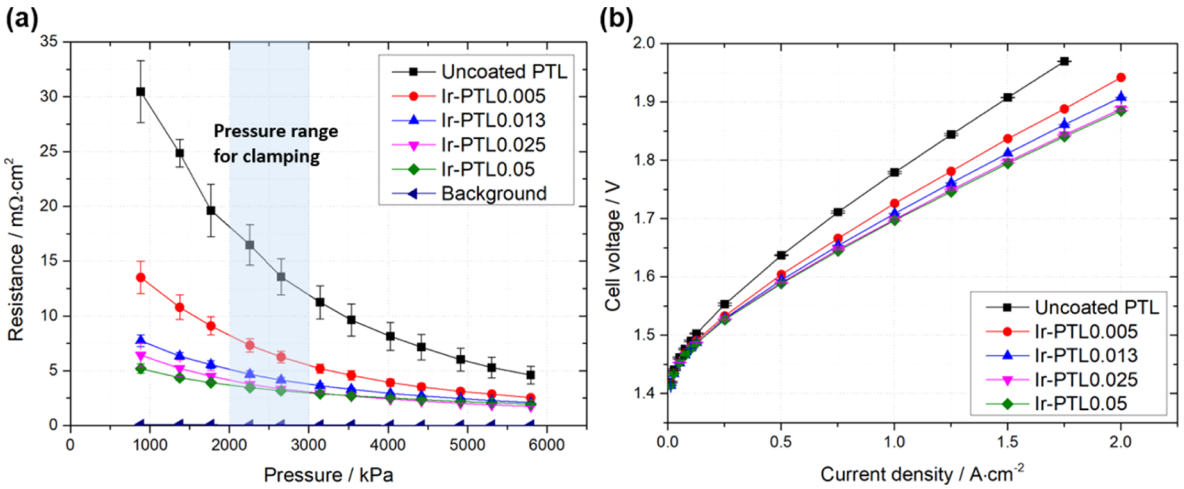

Figure 4. (a) Contact resistance of uncoated PTL, Ir-PTL0.005mg$_{Ir}$·cm^{-2}, Ir-PTL0.013mg$_{Ir}$·cm^{-2}, Ir-PTL0.025mg$_{Ir}$·cm^{-2}, and Ir-PTL0.05mg$_{Ir}$·cm^{-2}. Background: There is no sample between the two gold-coated plates. (b) Polarization curves of PEM water electrolyzer single cells assembled with Ir-PTL0.005mg$_{Ir}$·cm^{-2}, Ir-PTL0.013mg$_{Ir}$·cm^{-2}, Ir-PTL0.025mg$_{Ir}$·cm^{-2}, Ir-PTL0.05mg$_{Ir}$·cm^{-2}, and an uncoated PTL.

applied DC current at 4 A along with the measured voltage and Ohm's law.[9]

3. RESULTS AND DISCUSSION

3.1. Iridium on the PTL as a Protective Layer. The main components of a PEM water electrolyzer cell are presented in Figure 2a. The anode titanium-based PTL is a key component and serves to transport water to the anode's electrode, conduct electrons, and remove the produced oxygen. Figure 2b shows the conventional approach of Ir-coated PTLs using state-of-the-art CCM with 2.2 mg$_{Ir}$·cm^{-2} IrO_2 at the anode and 0.8 mg$_{Pt}$·cm^{-2} Pt/C at the cathode in a PEM water electrolyzer assembly. In Section 3.1, the effects of the Ir loadings on the Ir-PTLs will be investigated.

The PTLs were coated with 0.005, 0.013, 0.025, and 0.05 mg·cm^{-2} of iridium. Our recent research showed that the Ir layer coated on the Ti fiber is mostly in the metallic state and has an atomic ratio of 98:2 (Ir/O) prior to operation.[29] The elemental composition (wt %) of all of the Ir-coated PTLs measured using SEM–EDX is shown in Table S1. The concentration of Ir is nearly proportional to the sputtering time. The EDX mapping of Ir-coated PTLs in different Ir loadings revealed that the surfaces of the PTL fibers were all homogeneously covered with iridium (see Figure S1 in the Supporting Information). The brighter spots on the Ir mapping figures indicate an increase of the Ir concentration. This was also confirmed by the SEM images of the FIB-prepared cross sections of an Ir-PTL (Figure 3). Compared to the uncoated sample, a 7 nm-thick continuous and homogeneous Ir film can be observed in Ir-PTL0.005, which is the sample with the lowest degree of iridium loading. The FIB-prepared cross sections of Ir-PTLs in all the different Ir loadings show a continuous film (Figure S2 in the Supporting Information), which demonstrates that the entire surfaces of Ir-coated PTLs are homogeneously covered with Ir. The thicknesses of the iridium layers of Ir-PTL0.013, Ir-PTL0.025, and Ir-PTL0.05 are around 10, 13, and 27 nm, respectively, and the thickness of the Ir-PTLs increases nearly proportionally with the sputtering time.

To characterize the electrical conductivity properties of the PTLs, interfacial contact resistance (ICR) measurements were performed under different pressures. Figure 4a shows that the contact resistance of uncoated PTLs was higher throughout the entire compression ranges than all iridium-coated ones. This was caused by a naturally formed TiO_x surface-passivation layer due to the exposure to ambient air during the fabrication process and shelf storage.[9] For iridium-coated PTLs, the contact resistance gradually decreased with the increase in the Ir loading, which indicates that the amount of Ir, especially at low loadings, has a significant impact on the ICR. Moreover, Ir-PTL0.025 and Ir-PTL0.05 had identical resistances over the entire compression pressure, which is in accordance with the polarization curves and impedance spectra presented in Figures 4b and 5a (polarization curves and EIS will be discussed in the

https://doi.org/10.1021/acsami.0c20690
ACS Appl. Mater. Interfaces 2021, 13, 16182–16196

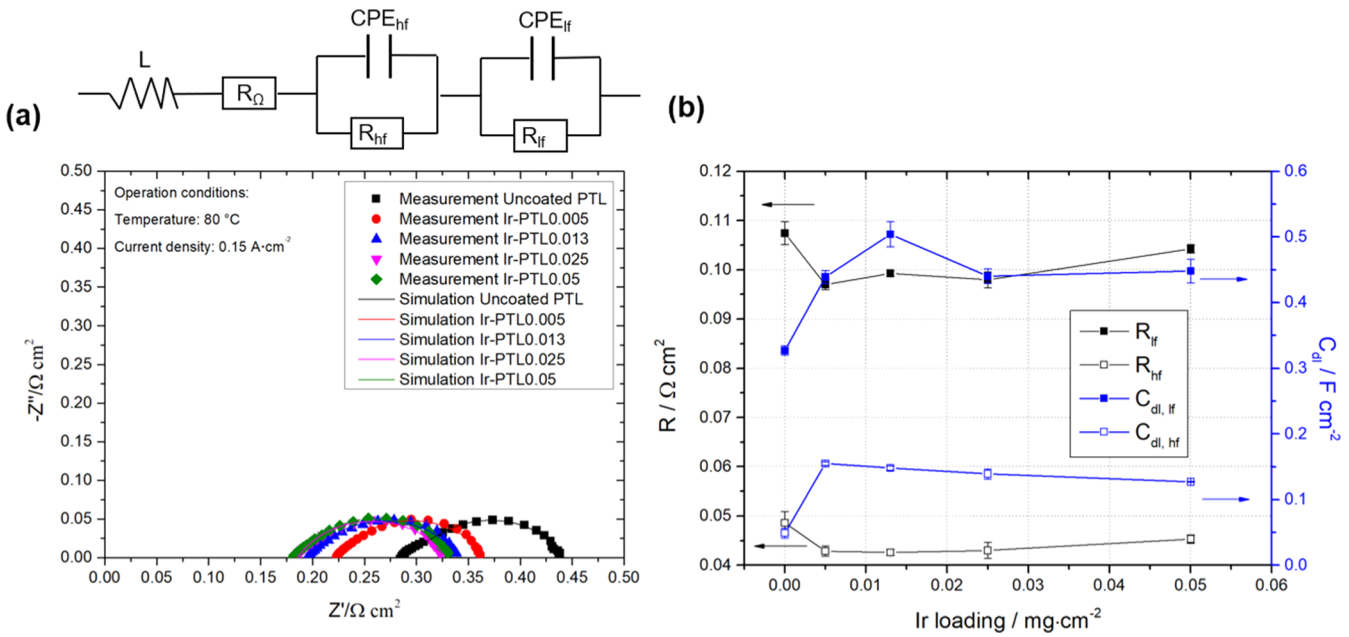

Figure 5. (a) EIS results at 0.15 A·cm^{-2} and equivalent circuit fitting; (b) kinetic resistances, R_{hf}/R_{lf}, and double layer capacitances, $C_{dl,hf}/C_{dl,lf}$, obtained from the fits of the impedance spectra shown in (a). The error bars represent the individual fitting errors of each value.

next section). At lower compaction forces (800−2000 kPa), there are overlaps of the standard deviation at lower compressions. The pressure used to clamp the test cells for electrochemical measurement is the shaded interval of the *X*-axis in Figure 4a, which was the recommended pressure range for assembling single PEM water electrolyzer cells.[33]

Figure 4b compares the cell performance of the uncoated and coated PTLs with different loadings of the Ir protective layer. Compared to the cell assembled with an uncoated PTL, the cell performances with Ir-PTL0.005 and Ir-PTL0.013 were improved by 53 and 70 mV at 1 A·cm^{-2}, respectively. The Ir-PTL0.025 and Ir-PTL0.05 samples exhibit an identical, improved cell performance with a significantly decreased cell voltage of, for example, 80 mV at 1 A·cm^{-2}. Clearly, there is a threshold of Ir loading value of around 0.025 mg$_{Ir}$·cm^{-2}. When the Ir loading corresponds to this, the cell's performance does not improve with the further increase in the Ir loading. The threshold loading value corresponds to the minimum amount of iridium coating required to obtain good contact and electronic conduction between the PTL and the electrode. The EDX results corresponded well with the cell performance and ICR results, which indicate that the higher coverage of iridium leads to lower contact resistance and so improved the cell's performance.

To investigate the effect of the protective layer's loading on the Ohmic resistance and electrochemical processes, electrochemical impedance spectra were recorded (Figure 5a). The Nyquist plots in the figure show strongly distorted semiarcs, which suggest the presence of two badly resolved processes with similar time constants, that is a smaller semiarc at high frequencies and a larger semiarc at low frequencies. Both semiarcs are associated with charge transfer in the rate-determining step of the OER and double-layer charging in the anode catalyst layer. However, the reason for the appearance of two semiarcs is still unclear. The electrochemical impedance spectra were modeled by means of the equivalent electrical circuit, as shown in Figure 5a. The equivalent circuit includes the Ohmic resistance, R_Ω, and two kinetic resistances, R_{hf} and R_{lf}, connected in parallel with the constant phase elements (CPEs), CPE_{hf} and CPE_{lf}, which result in two semiarcs. The fitting parameters of EIS of different PTLs at 0.15 A·cm^{-2} are shown in Table 2. The low overall fitting error of less than 1% results in a good match of the fitting curves and the experimental data.

By utilizing the Brug equation,[34,35] the approximate values of the double layer capacitances, $C_{dl,hf}$, and $C_{dl,lf}$, can be determined from the CPE values, their exponents *n*, and the corresponding resistances. The C_{dl} values shown in Table 2 are normalized to the geometric area. In the potential range where faradaic reactions such as OER take place, C_{dl} is not only proportional to the active surface but also depends on the coverage and properties of the adsorbed intermediates. Considering a roughness factor of several hundred up to thousands per milligram of catalyst, the C_{dl} values correspond to pseudo-double-layer capacitances of up to more than 100 μF/cm^2. These relatively high values are comparable with literature results: in case of OER on Pt in acid solutions, Conway and Liu observed a potential-dependent decrease of the pseudo-capacitance from values of more than 300 μF/cm^2 at *U*/RHE < 1.5 V down to values of less than 100 μF/cm^2 at potentials higher than 1.6 V.[36] These pseudo-capacitances are much higher than the capacity values in the range of some tens of μF/cm^2 obtained under non-faradaic conditions. This means that the pseudo-capacitance of the (OER) active area is higher than the double-layer capacitance of those parts of the catalyst/ionomer interface, which are less active or even inactive with respect to the OER. Less active areas are the outer parts of the catalyst layer close to the PTL. The reduced OER activity is caused by the resistance of proton transport in the catalyst layer. Inactive parts of the catalyst/ionomer interface have no contact with continuous paths of electron and/or proton conduction.

In any case, even the lowest Ir loading of the PTL causes a significant increase in the C_{dl}. If an increase in the active surface of the PTL would be the only reason for the higher C_{dl} values, a smaller effect would have been expected because the

https://doi.org/10.1021/acsami.0c20690
ACS Appl. Mater. Interfaces 2021, 13, 16182−16196

Table 2. Fitting Parameters of the EIS of the Ir-Coated PTLs at 0.15 A·cm^{-2}

sample	R_Ω/Ω cm^2	R_{lf}/Ω cm^2	R_{hf}/Ω cm^2	R_{DC}/Ω cm^2	CPE_{lf}/Ω^{-1} s^n cm^{-2}	CPE_{hf}/Ω^{-1} s^n cm^{-2}	n_{lf}/-	n_{hf}/-	$C_{dl,lf}$/F cm^{-2}	$C_{dl,hf}$/F cm^{-2}	$R_{DC}/R_{DC,uncoated}$/%
uncoated PTL	0.283	0.107	0.049	0.439	0.545	0.516	0.848	0.611	0.327	0.049	100
Ir-PTL0.005	0.222	0.097	0.043	0.362	0.648	0.672	0.877	0.707	0.439	0.155	82.5
Ir-PTL0.013	0.195	0.099	0.043	0.337	0.719	0.664	0.882	0.704	0.504	0.148	76.8
Ir-PTL0.025	0.183	0.098	0.043	0.324	0.642	0.659	0.88	0.696	0.440	0.139	73.8
Ir-PTL0.05	0.181	0.104	0.045	0.330	0.636	0.651	0.886	0.683	0.448	0.127	75.2

active area of the catalyst layer should be much larger by comparison to the sputtered Ir layer on the PTL. Rather, it can be assumed that the contact resistance plays an important role because the largest decrease of the ICR is obtained when impregnating the PTL with only 0.005 $mg_{Ir}\cdot cm^{-2}$. If a poor contact between the PTL and catalyst layer would impede the electron supply to Ir particles in the catalyst layer, the catalyst utilization and thus the active area and the double layer capacitance would decrease. Correspondingly, the catalyst utilization and the C_{dl} values increase when applying the Ir coating.

The relatively small effect of higher Ir loadings on the ICR would also explain why a further increase in Ir loading does not have a major impact on C_{dl}. The fitting error (see the error bars in Figure 5b) and approximate values derived from the Brug equation must also be taken into account. When impregnating the PTL with 0.005 $mg_{Ir}\cdot cm^{-2}$, the relative decrease of CPE and C_{dl} is larger for the high-frequency capacitance. This means that the influence of the impregnation is larger and suggests that the high-frequency semiarc may be associated with processes on Ir catalyst sites in the outer part of the catalyst layer and the PTL, respectively. However, the main impact of the ICR is on the Ohmic resistance. Thus, the largest part of the gain in performance when sputtering a protective layer of the Ir on the PTL is due to a considerable decrease in R_Ω (compare this with the high-frequency intercepts). In contrast, R_K, the kinetic resistance of OER that is the sum of the resistances R_{hf} and R_{lf}, decreases to a much smaller degree (compare the differences between the low- and high-frequency intercepts in Figure 5a).

In general, the Ohmic loss of a PEM water electrolyzer cell is the sum of the Ohmic resistances originating from the bulk resistances of each component, including the membrane, catalyst layers, PTLs, bipolar plate, and so forth, as well as the interfacial resistances between the components. Usually, most of the Ohmic loss stems from the membrane and interface between each component.[26] Because the same bulk components were used for the different MEAs and only the surface of the anode PTL was modified by the Ir coating, it is logical to conclude that the decrease in the Ohmic resistance was caused by that of the interfacial resistance of the PTL (see Figure 4a). Although the Ohmic resistance decreases almost linearly with decreasing interfacial resistance, the effect of Ir loading on R_Ω is nearly 1 order of magnitude higher than the effect of Ir loading on the ICR (compare this with the change in the R_Ω and ICR values in Tables 1 and 2). According to our previously published study, this result can be explained by the considerable difference in the ex situ conditions of the ICR tests and the electrolyzer cell's operating conditions regarding compression force, temperature, materials, and so forth.[25]

As is shown in Figure 6 and Tables 1, 2, the Ohmic resistance (R_Ω), ICR at 3000 kPa, and cell voltage at 1.5 A·cm^{-2} decrease exponentially with increasing Ir loading. At Ir loadings of 0.025 mg·cm^{-2} and above, R_Ω, the ICR and cell voltage remain virtually constant. Hence, concerning a reduction in the precious metal costs, the Ir loading of 0.025 mg·cm^{-2} would be sufficient to achieve the same cell performance as PTLs with a higher Ir loading. A decrease in the overall kinetic resistance R_K for each current density can be calculated from the overall decrease of the cell voltage (Table 2). The contribution of the sputtered Ir layers to the overall performance can be calculated from the DC resistance, R_{DC}, which is the sum of the Ohmic and the kinetic resistances, that

https://doi.org/10.1021/acsami.0c20690
ACS Appl. Mater. Interfaces 2021, 13, 16182−16196

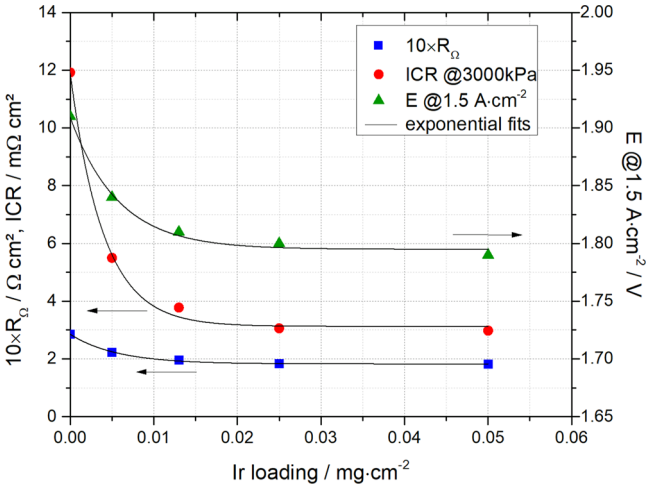

Figure 6. Ir loading of the Ir-PTL ($mg_{Ir}·cm^{-2}$) vs the cell voltage (V) at 1.5 $A·cm^{-2}$; 10 × Ohmic resistance@0.15 $A·cm^{-2}$ ($Ω·cm^2$) and ICR ($mΩ·cm^2$)@3000 kPa.

is, $R_{DC} = R_Ω + R_{hf} + R_{lf} = R_Ω + R_K$. This is evident if R_{DC} of each sample is normalized to R_{DC} of the uncoated sample. The resulting percentage values are shown in Table 2. Compared to an uncoated sample, the overall DC resistance of Ir-coated PTL0.025 decreased by about 26%.

As mentioned above, most part of the gain in performance is due to the decrease in Ohmic resistance. With increasing current density, the ohmic contribution of the DC resistance, $R_Ω$, increases more strongly than the kinetic part, R_K. However, the small decrease of R_{hf} and R_{lf} cannot be neglected, as Figure 5b shows. Both resistances decrease by about 10% when increasing the Ir loading from 0 to 0.025 $mg·cm^{-2}$. Together, they contribute approximately 13% of the overall decrease in the total resistance (87% is due to the decrease in $R_Ω$). This additional gain in performance can be explained by the electrochemical activity of the Ir coating layer toward the OER, which is demonstrated in Figure 7a and will be discussed in the next section. It should however be noted that the additional OER activity of the Ir-coated PTL is an effect that is observed in particularly small current densities. This is because with increasing current density, the Ohmic resistance becomes increasingly dominating. Moreover, the resistance of proton

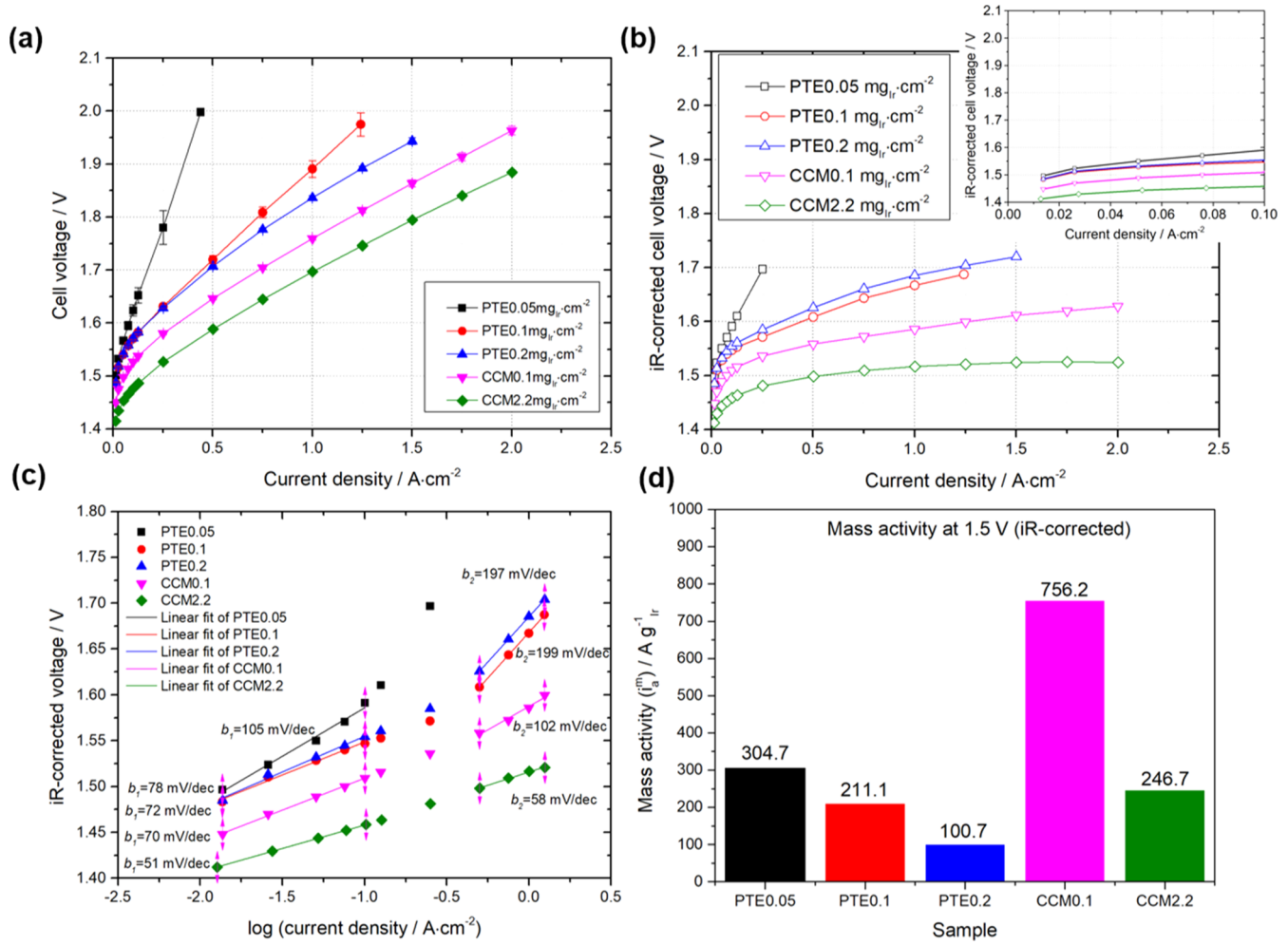

Figure 7. (a) Polarization curves of single PEM water electrolyzer cells assembled with PTE0.05, PTE0.1, PTE0.2 as the anodic catalyst layer and 0.8 $mg·cm^{-2}$ Pt at the cathode [reference: CCM0.1 (0.1 $mg·cm^{-2}$ IrO_2 and 0.8 $mg·cm^{-2}$ Pt) and CCM2.2 (2.2 $mg·cm^{-2}$ IrO_2 and 0.8 $mg·cm^{-2}$ Pt)]; (b) cell voltage corrected by the high frequency resistance (HFR); inset: kinetic region of the *iR*-free cell voltage; (c) Tafel plot of the *iR*-corrected voltage data from (b) for different anode loadings of iridium coating. The Tafel slope is obtained from a linear fit of the values between 0.0125 and 0.1 $A·cm^{-2}$; (d) mass activity at 1.5 V (*iR*-corrected).

https://doi.org/10.1021/acsami.0c20690
ACS Appl. Mater. Interfaces 2021, 13, 16182−16196

conduction in the anode catalyst layer increases and the OER proceeds mainly in the inner part of the catalyst layer adjacent to the Nafion membrane.

3.2. Iridium on the PTL as Both the Protective Layer and PTEs. In order to (1) explain the additional gain in performance by the reduction in the kinetic resistances and (2) more importantly, to investigate the OER activity of the Ir-coated PTL and whether it is beneficial to increase the cell performance, the Ir-coated PTLs were assembled with a half-side CCM without an IrO_2 catalyst layer on the anode side, but with 0.8 $mg_{Pt}\cdot cm^{-2}$ Pt on the cathode side, on the Nafion membrane (Figure 2c). The Ir-coated PTLs in this section are referred to as PTEs. The performances of two reference CCMs with 0.1 or 2.2 $mg_{Ir}\cdot cm^{-2}$ are compared with those of three PTEs with 0.05, 0.1, and 0.2 $mg_{Ir}\cdot cm^{-2}$ of iridium. When the PTE is pressed on the soft Nafion membrane, the latter will penetrate into the porous Ir-coated PTL to some extent (and vice versa), supposedly forming a three-phase boundary of the Ir, Nafion membrane, and gas phase, which represents the active area. However, the electrochemically active area of the PTE samples shall be significantly smaller than that of a normal catalyst layer because the (pore) structure is much coarser and there is no additional ionomer to extend the catalyst/ionomer contact area (compare this with the top view of the PTE and CCM samples in Figure 8).

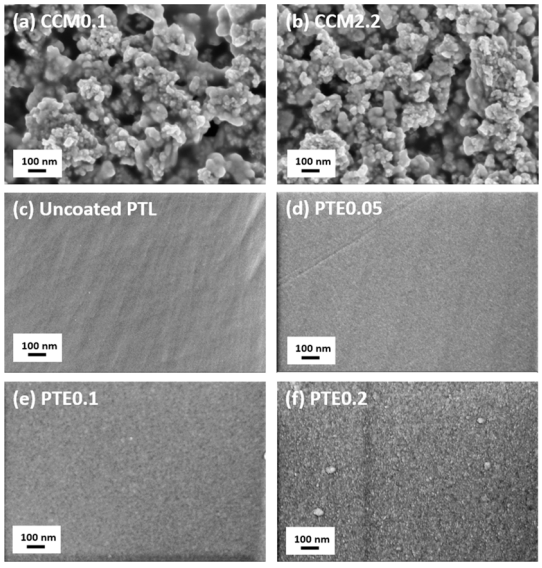

Figure 8. High-resolution SEM images of (a) CCM0.1$mg_{Ir}\cdot cm^{-2}$; (b) CCM2.2$mg_{Ir}\cdot cm^{-2}$; (c) an uncoated PTL; (d) PTE0.05$mg_{Ir}\cdot cm^{-2}$; (e) PTE0.1 $mg_{Ir}\cdot cm^{-2}$; and (f) PTE0.2 $mg_{Ir}\cdot cm^{-2}$.

Figure 7a shows that electrochemical activity is observed for all the PTE samples although their cell performance was, as expected, lower than that of the reference CCMs. Compared to the PTE samples, both reference CCM samples feature a higher active area. This is especially apparent in a comparison of the CCM0.1 and PTE0.1 samples: despite the same Ir loading, the anode catalyst layer in the CCM0.1 showed a significantly better performance than the sputtered Ir layer. For the PTE samples, the cell performance increased significantly by increasing the Ir loading from 0.05 to 0.1 $mg_{Ir}\cdot cm^{-2}$ but changed only minimally when the loading was further enhanced (Figure 7a). This suggests an asymptotic dependency of the active area versus the Ir loading of the PTE, with a saturation value near the loading of 0.1 $mg_{Ir}\cdot cm^{-2}$. Because the OER rate of the PTE samples is smaller than that of the CCM samples, the OER of the PTE samples dominates the overall performance even more than in the case of normal CCMs. Therefore, the potential differences can be solely attributed to the anode reaction. For example, the onset potential of the PTE samples is approximately 50 mV higher than that of the CCM0.1 and about 100 mV higher than that of CCM2.2. This can be explained with reference to the strongly different active areas and intrinsic activities. In their recent publication, Zhao et al.[37] reported an electrochemical surface area (ECSA) of 1.81 m^2 for an PEM electrolyzer MEA with an Ir oxide catalyst layer on the anode side and an area of 25 cm^2, which corresponds to a roughness factor of 724. Although we have no ECSA data for the PTE samples, roughness factors of much more than 10 are very unlikely because only those parts of the sputtered Ir oxide layer which are in contact with the Nafion membrane can be active toward OER. Therefore, the active area of the CCM anode catalyst layer must be orders of magnitude higher than that of the PTE samples, which results in a corresponding decrease in the apparent exchange current density of the OER/oxygen reduction reaction (ORR).

In order to eliminate the influence of Ohmic resistances, the *iR*-corrected cell voltages versus the current density are plotted in Figure 7b. The 50−250 mV lower voltages of reference samples CCM0.1 and CCM2.2 compared to those of PTE0.1 and PTE0.2 can partly be attributed to the above-mentioned shift in the onset potential due to the higher active surface area. Tafel slopes b_1 and b_2 were determined in the low and high current density ranges, apart from the PTE0.05 sample, where high current densities could not be achieved. At low current densities, the CCM2.2 sample shows an apparent Tafel slope of 51 mV/dec, which is close to the intrinsic OER Tafel slope of 40 mV/dec proposed for a rate-determining second charge-transfer step (deprotonation of adsorbed OH, i.e., $OH_{ad} \rightarrow O_{ad} + H^+ + e^-$) and within the range of apparent Tafel slopes of 38−55 mV/dec reported by Slavcheva et al.[38] The same is true for high current densities, where CCM2.2 shows a b_2 value of 58 mV/dec, which is close to the b_1 value and does not indicate a change in the rate-determining step (r.d.s.). In contrast, the CCM0.1 sample shows a pronounced increase in the Tafel slope from 70 to 102 mV/dec. The b_2 value of 102 mV/dec is close to the intrinsic Tafel slope of 120 mV predicted for a rate-determining first charge-transfer step (deprotonation of the adsorbed water, i.e., $H_2O_{ad} \rightarrow OH_{ad} + H^+ + e^-$). Thus, the pronounced change in the Tafel slope for the CCM0.1 sample may be interpreted as a change in the rate-determining deprotonation step of water instead of OH. However, different catalyst sites are present in the catalyst layers, including crystalline and amorphous IrO_x phases or surface and subsurface sites on/inside the IrO_x layers. As pointed out by Slavcheva et al.[38] and Marshall et al.,[39] the apparent Tafel slopes may be regarded as an average value originating from different catalyst sites over which the OER may proceed via different mechanisms, r.d.s.'s or even different charge-transfer coefficients deviating from 0.5.

The Tafel slopes (b_2) of the PTE0.1 and PTE0.2 samples in the high current density range are apparently high, in the range of 110−220 mV/dec, as obtained by Slavcheva et al.[38] As the b_2 value is nearly twice as high as the value predicted for a rate-determining first charge-transfer step, it is highly questionable as to whether this Tafel slope can be ascribed for a rate-determining deprotonation of adsorbed water. Therefore, there

https://doi.org/10.1021/acsami.0c20690
ACS Appl. Mater. Interfaces 2021, 13, 16182−16196

must be other reasons that explain the high apparent Tafel slopes at low Ir loadings. Although the *b* values were determined from linear fits, it should be noted that the Tafel slopes tend to continuously increase at current densities higher than 0.1 A·cm^{-2}, except for the CCM2.2 sample. In light of the above discussion, the following features of Figure 7b,c must be explained

(i) The difference in the *iR*-corrected cell voltages of PTE0.1, PTE0.2, and CCM0.1 increases steadily by increasing the current density, which corresponds to a considerable increase in the Tafel slope.

(ii) The same is true when comparing the PTE0.05 and PTE0.1 samples: the voltage difference increases by up to 126 mV@0.25 A·cm^{-2} (and would further increase at higher current densities) when decreasing the Ir loading from 0.1 to 0.05 mg·cm^{-2}.

(iii) There is only little difference in the (*iR*-corrected) cell voltages and Tafel slopes of the PTE0.1 and PTE0.2 samples and virtually no difference at low current densities.

(iv) The *iR*-corrected (and non-corrected) cell voltages of the PTE samples at low current densities and their onset potentials of OER little depend on the *iR*-loading (see the kinetically dominated current region in the inset picture).

Ad (i) and (ii):

In the case of the low Ir loadings, Bernt et al. obtained an unexpectedly high increase in the *iR*-free cell voltage as well, leading to higher Tafel slopes.[40] They explained this effect by reference to an inhomogeneous distribution of catalyst particles in very thin catalyst layers (≈1 μm) on the membrane in combination with a rough pore structure in the PTL. This leads to electronically poorly accessible catalyst particles on the membrane surface and means lower utilization of the catalys, as well as higher Ohmic resistance. Clearly, there is a substantial difference between their samples and ours: the Ir films are sputtered on the PTL and not prepared on the membrane. Thus, in contrast to their model, this means a poor accessibility of protons instead of electrons: a lower utilization would be due to the poorly utilized Ir sites, which have no contact with the Nafion membrane. These sites may be located on the surface and/or in the subsurface region of the sputtered Ir layers. In the case of the former, there would be access of water via the voids between the Ti fibers. In the latter case, cracks or small pores in the Ir films would be necessary to enable access of water and the removal of oxygen and protons to/from subsurface catalyst sites. For the $Ru_{0.7}Ir_{0.3}O_2$ catalyst, Xu and Scott observed an additional charge in the cyclic voltammograms at low scan rates, which they attributed to the utilization of catalyst sites beneath the surface through slow proton diffusion.[41]

Slavcheva et al. have shown that the morphology, performance, and utilization of sputtered Pt layers depend on the sputtering conditions, especially the Ar pressure and sputtering time, which affects the Pt loading and film thickness.[42] Increasing Pt loading leads to an increase in the thickness, surface roughness, and voids of/in the sputtered Pt layers. This in turn increases the number and accessibility of subsurface catalyst and adsorption sites on the Pt surface and thus the active surface area, the ORR performance, and catalyst utilization. Higher catalyst utilization in the case of the PTE0.1 and PTE0.2 samples may explain the lower Tafel slopes compared to the PTE0.05 sample. Moreover, the surface roughness of the Ir layers increases with increasing Ir loading. This effect, together with a higher number of subsurface sites, should lead to a higher overall number of active Ir sites and thus to better performance. According to Slavcheva et al.,[42] the utilization of Pt decreases at film thicknesses higher than 125 nm because of the limited penetration depth of the oxygen species. Thus, there seems to be a "utilization maximum" at a certain film thickness that should depend on the type of catalyst, the sputtering conditions, the morphology of the sputtered films, and the electrochemical reaction, including the type of diffusing species (small atoms/ions such as H/H^+ or molecules such as H_2O and O_2). In a previous paper, Slavcheva et al. identified a decreasing utilization of sputtered Ir oxide layers with increasing film thicknesses.[38] However, their lowest film thickness was 250 nm, that is, about three times higher than that of the PTE sample with the highest Ir loading of 0.2 mg·cm^{-2} and two times higher than the critical Pt film thickness at maximum utilization. If the very thin Ir films prepared in this work have a thickness below the critical value corresponding to the maximum utilization, an increasing utilization may be the reason for the pronounced decrease in the Tafel slope when increasing the Ir loading from 0.05 to 0.1 mg·cm^{-2}.

An increase in utilization is associated with an extension of the active area and vice versa. This is important because the current densities shown in Figure 7 are normalized to the geometric area and not to the active, utilized one. If the catalyst utilization and active area decrease with increasing current, this would lead to a higher increase in the OER overpotential than that expected for an active area independent of the current density. In the case of the CCM2.2 sample, the relatively high Ir loading and large triple phase boundary resulting from the microporous structure and the addition of ionomers causes only a small increase in the Tafel slope at higher current densities. As was expected, the effect is more pronounced when decreasing the catalyst loading and thus the active area of the CCM by more than 1 order of magnitude (see the CCM0.1 sample). The highest increase in the Tafel slope is observed for the PTE samples because at the same catalyst loading level, the sputtered Ir layers have a smaller active area than the microporous catalyst layers and so there is no "'buffer effect" of a large triple phase boundary, especially at high current densities. In the case of the PTE0.05 sample, a dramatic increase in cell voltage is observed. Moreover, the continuous increase in the slope even starts at current densities below 0.1 A·cm^{-2} and apparent slopes of more than 250 mV/dec are reached at higher current densities.

In essence, an extension of the reaction zone could be achieved by water, oxygen, and proton diffusion in the catalyst/membrane interface or in the catalyst/pore interface. A slow diffusion of water and oxygen in small pores or gaps may also cause an additional mass transport/diffusion resistance. An extension of the reaction zone to the catalyst/pore interface by, for example, a slow surface diffusion of protons would only play a role if the surface properties of the Ir layers would depend on the film thickness, which in turn could influence the surface diffusion coefficient of the protons. In any case, an increase in surface roughness with increasing film thickness is evident from Figure 8. The subsurface Ir sites in the sputtered layers can only be utilized if cracks or pores are present. However, the FIB images shown in Figure S3 in the Supporting Information reveal dense and homogeneous Ir

https://doi.org/10.1021/acsami.0c20690
ACS Appl. Mater. Interfaces 2021, 13, 16182−16196

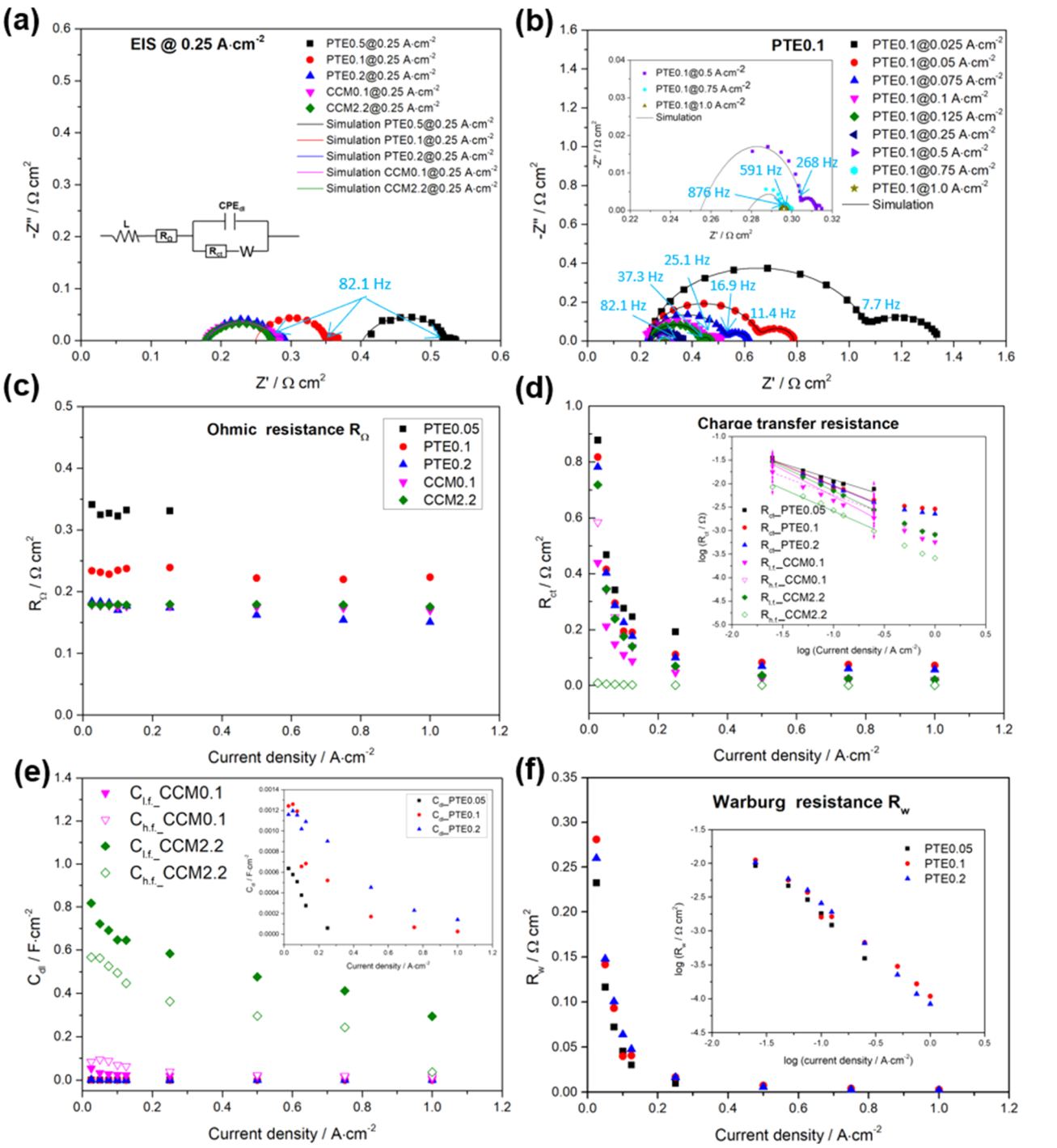

Figure 9. (a) EIS results at 0.25 A·cm^{-2} and equivalent circuit fitting; (b) EIS results of PTE0.1 at different current densities and equivalent circuit fitting; inset panel: EIS results of PTE0.1 at 0.5, 0.75, and 1.0 A·cm^{-2}; (c) fitted Ohmic resistance at different current densities; (d) charge-transfer resistance at different current densities; inset panel: logarithmic plots of charge-transfer resistance; (e) capacitance (C_{dl}) at different current densities; (f) Warburg resistance (R_w). All of the EIS measurements were performed at 80 °C.

layers without any porosity. This excludes the accessibility of subsurface sites for water or oxygen. Nevertheless, differentially oriented crystallites (grains) of Ir are visible, which might enable the slow diffusion of protons along the grain boundaries.

Because the *iR*-corrected polarization curve of the CCM2.2 sample shows only a slight increase in the Tafel slope at higher current densities (see Figure 7c), a mass transport limitation of, for example, water in the pores of the anode catalyst layer does not play a considerable role. This is supported by the polarization curve of the CCM0.1 sample: because their anode catalyst layer is much thinner, a possible mass transport effect in the pores should be even smaller and there should be virtually no increase in the Tafel slope at higher current densities. Indeed, the converse is true. In the case of the PTE samples, a slow mass transport of water and oxygen in the interface of the Ir-sputtered Ti fibers and the Nafion membrane has to be considered. For example, the transport

https://doi.org/10.1021/acsami.0c20690
ACS Appl. Mater. Interfaces 2021, 13, 16182−16196

of water to the active sites might be hampered by trapped oxygen gas bubbles in the Ir/Nafion interface, resulting in higher Tafel slopes. Because a change in Ir loading leads to a change in the structure and properties of the Ir surface (see, e.g., Figure 8) and the Ir/Nafion interface, this in turn should influence the mass transport in the interface and thus the Tafel slope. In fact, the slope of the polarization curves increases significantly if the current density increases and the Ir loading decreases. Conversely, there is no reason why very thin Ir layers should influence the mass transport in the large voids of the PTL. If the latter effect would be the dominant mass transport process, the Tafel slope would be independent of the Ir loading, which is not the case. Hence, a possible diffusion limitation can only result from the diffusion of species such as water and oxygen in the membrane/catalyst interface or a slow surface diffusion of protons on Ir sites that have no contact with the proton conducting membrane.

Ad (iii) and (iv):

As stated above, the surface of the sputtered Ir layers becomes rougher when increasing the Ir loading (Figure 8), leading to a larger membrane/catalyst interface and, considering an extension of the active area into the membrane/catalyst interface, a higher electrochemically active area and thus to better performance. A similar effect has been reported by Slavcheva et al.[42] and Kang et al.[30] in the case of sputtered Pt thin films. At small film thicknesses similar to ours, the roughness value increases by approximately a factor of 2 when doubling the Ir loading and thus the film thickness.[42] If the active area is also doubled when, for example, increasing the Ir loading from 0.05 to 0.1 mg·cm^{-2}, the voltage would only decrease by ≈14 mV, assuming an intrinsic Tafel slope of 47 mV (see eq 3 in Bernt et al.).[40] These small differences in voltage explain why the onset potentials of the OER of the PTE samples little depend on the Ir loading. Kang et al. observed a decrease in performance at the highest levels of Pt film thickness and roughness. They explained this unexpected effect on the basis of a decrease in the number of contact points between the catalyst particles and membrane due to the coarse surface structure.[30] Another explanation lies in a decreasing extension of the reaction zone because of the closer contact of a rougher catalyst surface and the membrane, which may "close" possible diffusion paths for water and oxygen. In any case, the mutual compensation of two opposing effects may explain why the polarization curves of the PTE0.1 and PTE0.2 samples are almost identical at low current densities. Obviously, the *iR*-corrected cell voltage of PTE0.2 at higher current densities is slightly higher than that of PTE0.1. A tentative explanation can be derived from the model of Kang et al. (see above). Because the surface properties of the sputtered Ir layers will have a great impact on the properties of the Ir/Nafion interface, it appears likely that an unfavorable change in surface and interface properties will have a larger impact on the OER kinetics than on the Ohmic resistance. If, for example, an increase of the Ir loading from 0.1 to 0.2 mg/cm^2 increases the Ohmic resistance a little, but increases the resistance of the OER kinetics to an even larger extent, the observed effect would be explainable.

If the OER current densities shown in Figure 7b,c are normalized to the Ir loading, the resulting mass activities depend very much on the chosen *iR*-corrected voltage as well as the actual active area and utilization of the Ir catalyst. As an example, the calculated mass activities calculated at 1.5 V (*iR*-corrected) are shown in Figure 7d. Because the microporous structure of the catalyst layers in the CCM samples allows much better utilization of the Ir catalyst, the mass activity of a CCM sample is higher than that of a PTE sample with the same catalyst loading. This is indeed the case if one compares the mass activities of, for example, CCM0.1 (545 A g^{-1}) and PTE0.1 (211 A g^{-1}). The lower mass activity of CCM2.2 compared to CCM0.1 can simply be explained by the fact that especially in the case of thick catalyst layers, the outer part of the CCM anode catalyst layer close to the PTL is less utilized. For a similar reason, the mass activity of the PTE samples decreases when increasing the Ir loading from 101 to 305 A g^{-1}: because only the Ir sites at the surface of the Ir films are active for OER and thus the inner Ir sites are non-utilized and wasted, higher mass activities are achieved with thin Ir layers. As explained above, a small active surface in combination with low catalyst utilization leads to smaller and smaller current densities when increasing the cell voltage. Therefore, the mass activity of the PTE samples relative to that of the CCM samples correspondingly decreases. This is evident from a comparison of the mass activities of CCM0.1 and PTE0.1: for an *iR*-corrected cell voltage of 1.5 V (see above), the ratio of mass activities is 3.6 (756:211 A g^{-1}) and increases to a ratio of 4.0 (1827:460 A g^{-1}) at 1.525 V. If a critical *iR*-corrected cell voltage is exceeded (here: 1.544 V), the mass activity of the PTE0.05 sample falls even below that of the PTE0.1 sample. The intersection of the mass activities of the PTE0.05 and PTE0.1 samples at 1.544 V can be seen in the semilogarithmic plots of the *iR*-corrected cell voltage versus the logarithm of the mass activity (see Figure S4 in the Supporting Information). The decrease in mass activity with decreasing Ir loading was also reported by Bernt et al.[40]

Because the structure and properties of the active ionomer-free Ir catalyst layer in the PTEs significantly differ from those of common anode Ir catalyst layers with ionomers, the impedance spectra should be different as well. This is indeed the case, as is shown in Figure 9a,b with the examples of 0.25 A·cm^{-2} and PTE0.1 at different current densities (more EIS results can be found Figure S5 in the Supporting Information). Contrary to the spectra shown in Figure 5a, two distinct semiarcs with very different time constants are observed (time constant $\tau = R \times C$ is reciprocal to the peak frequency of a semiarc). Using the same equivalent circuit as for the PTL samples, the capacitance fit values of the low frequency (l.f.) semiarc were surprisingly higher than those obtained for the CCM samples. However, the (pseudo) double-layer capacitance of the electrodes is proportional to the electrode/electrolyte interface. Because the latter was significantly higher for the CCM anode catalyst layer compared to the PTE, a much lower capacitance is expected for the PTE samples. Hence, an interpretation of the l.f. semiarc as a charge-transfer resistance in parallel to double-layer capacitance is not appropriate. However, it can be assumed that the small active area of the PTEs may be extended by, for example, the diffusion of water and oxygen to/from Ir particles in the catalyst/membrane contact. This could either be a diffusion in small pores between the Ir/IrO_x surface and the Nafion membrane or within the membrane itself. Therefore, it seems reasonable to correlate the l.f. semiarc with a diffusion process and thus to attribute the high frequency (h.f.) semiarc to the OER charge-transfer process in parallel with the double-layer capacitance. An appropriate equivalent circuit is shown in the inset of Figure 9a. Apart from the h.f. cable inductance and the Ohmic resistance, this consists of a charge-transfer resistance,

https://doi.org/10.1021/acsami.0c20690
ACS Appl. Mater. Interfaces 2021, 13, 16182−16196

R_{ct}, a double-layer capacitance represented by a CPE element and a finite Warburg element representing the diffusion process. Because the charge-transfer process on the PTE anode occurs at much higher frequencies than that of the CCMs, the h.f. charge transfer semiarc of the CCMs is likely masked by the unavoidable inductive effects. This might explain why only one semiarc associated with the charge transfer is observed for the PTE samples.

For the PTE samples, the semiarc associated with the OER charge-transfer process appears at frequencies more than 2 orders of magnitude higher than those of the CCM samples. This can be explained as follows: because the (differential) double-layer capacitance is roughly proportional to the catalyst/ionomer interface and the latter decreases by more than 1 order of magnitude when substituting a normal CCM catalyst layer by an Ir sputtered PTE catalyst layer, the C_{dl} value should correspondingly decrease. The charge-transfer resistance R_{ct} represents the slope of the *iR*-corrected polarization curve in the kinetically controlled region and should therefore increase proportionally with the Tafel slope b_1 determined in the low current density range. As can be seen in Figure 7b,c, the slopes of the PTE 0.1 and 0.2 samples are somewhat higher than those of the CCM2.2 sample but close to that of the CCM0.1 sample. This results in similar R_{ct} values and, respectively, diameters of the dominating semiarc of the CCMs and the h.f. semiarc of the PTE samples (see Figure 9a,b). Hence, the significant decrease in the double-layer capacitance dominates the time constant of the h.f. semiarc and leads to the pronounced shift to higher frequencies.

The fit results of the Ohmic resistance as a function of the current density are shown in Figure 9c. As expected, R_Ω only slightly depends on *j*. In general, a higher contact area between the electrode and membrane should suppress in-plane proton transport beneath the membrane surface and thus decrease the Ohmic resistance. It turns out that the Ohmic resistance of the PTE samples decreases with increasing Ir loading. This can be explained by higher surface roughness, which leads to better contact between the catalyst layer and membrane. At the same time, the abovementioned effect of a decreasing number of contact points can be excluded. If considering the dependence of the contact resistance from the Ir loading shown in Figure 4a, a much smaller effect on the Ohmic resistance would be expected. However, the contact of the PTL with the wet, swollen Nafion membrane will differ from the contact PTL/gold. The contact resistance could also be the reason for the higher R_Ω value of the CCM samples compared to the PTE0.2 sample: because the CCM samples imply the anode catalyst layer, that is, two functional electrode layers (PTL + CL) instead of one such as the PTE samples, additional contact resistance must be considered.

The exponential decrease in R_{ct} (see Figure 9d) corresponds to the Butler–Volmer kinetics of the OER, that is, an exponential increase in the OER current density with increasing overpotential (increasing *iR*-corrected cell voltage). The increase of R_{ct} ($R_{ct} = R_{hf} + R_{lf}$ in case of the CCMs) is in the following order: CCM2.2 < CCM0.1 ≈ PTE0.2 ≈ PTE0.1 < PTE0.05, which follows the order of the b_1 values, as explained above. The decay in the double-layer capacitance with increasing current density (see Figure 9e) can be explained by a decreasing utilization and active area, as is noted above. In the case of the CCM samples, this effect is less pronounced because of the large triple phase boundary, which is especially true for the CCM2.2 sample. In contrast, the C_{dl} values of the PTE samples dramatically decrease by 1–2 orders of magnitude. For the same reason, the capacitance decay becomes stronger, as the Ir loading of the PTE samples decreases. It should be noted that the Brug equation used for the calculation of C_{dl} only provides approximate values and the error becomes larger with increasing deviation of the exponents *n* from one. Because the *n* values decrease with increasing current for all samples (see Figure S6a in the Supporting Information), this certainly has a substantial impact on the observed decay of the capacitance. However, even if the *n* value would be independent of the current density, the capacitance decreases with increasing current density. For comparison, the *n* and CPE values versus the current density are shown in Figure S6 in the Supporting Information. Whereas the CPE values of the PTE samples tend to decrease, even though not quite as much as their corresponding capacitances, the CPE values of the CCM samples exhibit no clear tendency.

As is stated above, the spectra of the PTE reveal a low-frequency semiarc associated with a diffusion process. The strong decrease in the diffusion resistance R_w with increasing current density (see Figure 9f) may be perplexing at first glance as it would normally show the opposite behavior. For instance, the mass transport resistance associated with the transport of water in the space between the Ti fibers or the pores of common anode catalyst layers would increase with the current density and can be excluded here. However, it must be considered that the low-frequency diffusion process and R_w only occurs if the reaction zone is extended at the expense of additional resistance due to the diffusion of active species such as water, oxygen, and protons in the catalyst/membrane interface. With increasing current density, the OER occurs closer to the triple phase boundary and the diffusion of species in the membrane/catalyst interface becomes ever less important. A definite identification of the species associated with the diffusion limitation (protons, water, and/or oxygen) is not possible on the basis of the results presented here. However, the fast bulk diffusion of protons in the fully hydrated membrane via the Grotthuss mechanism ($D_{H^+} \approx 10^{-4}$ cm^2 s^{-1},[43]) would contribute to the Ohmic resistance. Only a slow surface diffusion of protons on Ir sites that have no contact with the Nafion membrane would cause additional diffusion resistance. The most probable reason for the appearance of the low-frequency semiarc is the slow diffusion of water and oxygen at the interface of the Ir-sputtered Ti fibers and Nafion membrane.

It should be noted that the decrease in the Warburg resistance with increasing current density is not due to the fitting model. A similar decrease would be obtained if the low frequency process was fitted with a simple (*R*-CPE) combination, that is, an equivalent circuit with two (*R*–CPE) combinations in series. In case of the PTE samples, two distinct semiarcs with well-separated time constants are obtained. An appropriate impedance model must contain elements that best represent parameters of the electrochemical processes taking place in the system investigated. In our case, the most probable interpretation of the low-frequency process is a diffusion process in the Ir oxide/membrane interface, as explained above.

4. CONCLUSIONS

In this study, titanium-based PTLs were sputter-coated with iridium as protective layers. We confirmed the specific

https://doi.org/10.1021/acsami.0c20690
ACS Appl. Mater. Interfaces 2021, 13, 16182–16196

thicknesses of the iridium layer with different loadings and found that even the lowest loading of 0.005 mg·cm^{-2} reduces the contact resistance between the PTLs and catalyst layers considerably. The Ir protective layer not only decreases the Ohmic resistance, which is the biggest portion of the gain of performance, but also decreases the resistances associated with charge transfer because it is electrochemically active regarding the OER. The Ir-coated PTL, with only 0.025 mg·cm^{-2} of Ir, is sufficient to show the identical cell performance as the Ir-coated PTL with the higher loading. The cell's performance no longer depends on the loading when the Ir loading is above this value, which is 40 times less compared to the Au or Pt loading typically used for protective layers in current commercial electrolyzers. Compared to an uncoated PTL, the voltage loss of the cell with only 0.025 mg_{Ir}·cm^{-2} to the PTL is smaller by 80 mV at 1.0 A·cm^2. The significant increase in the OER onset potential and of the apparent Tafel slope, especially at low-Ir loading, is attributed to a decrease in the active area and utilization of the catalyst. If Ir-coated PTLs are pressed onto the Nafion membrane, another mass transport process has to be considered, which is most probably the slow diffusion of oxygen and water in the IrO_x/Nafion interface. This work not only demonstrates an easy and scalable approach to reducing interface resistivity between the PTL and the electrode but also may provide a promising means to develop catalyst layers for low-temperature PEM water electrolyzers. Future work will be performed to optimize the iridium layer properties, such as optimizing the sputtering parameters, the triple phase boundary of Ir, Nafion, and the gas phase to further increase the catalyst utilization and active area.

■ ASSOCIATED CONTENT

Supporting Information

The Supporting Information is available free of charge at https://pubs.acs.org/doi/10.1021/acsami.0c20690.

EDX mapping of Ir of Ir-coated PTLs, SEM images of FIB-prepared cross-sectional image of Ir-coated PTLs, and additional electrochemical data (PDF)

■ AUTHOR INFORMATION

Corresponding Author

Marcelo Carmo − *Institute of Energy and Climate Research, IEK-14: Electrochemical Process Engineering, Forschungszentrum Jülich GmbH, 52425 Jülich, Germany; Mechanical and Materials Engineering, Queen's University, Kingston, ON K7L 3N6, Canada;* orcid.org/0000-0002-0186-317X; Email: m.carmo@fz-juelich.de

Authors

Chang Liu − *Institute of Energy and Climate Research, IEK-14: Electrochemical Process Engineering, Forschungszentrum Jülich GmbH, 52425 Jülich, Germany; Faculty of Mechanical Engineering, RWTH Aachen University, 52062 Aachen, Germany*

Klaus Wippermann − *Institute of Energy and Climate Research, IEK-14: Electrochemical Process Engineering, Forschungszentrum Jülich GmbH, 52425 Jülich, Germany;* orcid.org/0000-0002-5489-9280

Marcin Rasinski − *Institut für Energie- und Klimaforschung—Plasmaphysik (IEK-4), Forschungszentrum Jülich GmbH, 52425 Jülich, Germany*

Yanpeng Suo − *Institute of Energy and Climate Research, IEK-14: Electrochemical Process Engineering, Forschungszentrum Jülich GmbH, 52425 Jülich, Germany; RWTH Aachen University, 52062 Aachen, Germany*

Meital Shviro − *Institute of Energy and Climate Research, IEK-14: Electrochemical Process Engineering, Forschungszentrum Jülich GmbH, 52425 Jülich, Germany;* orcid.org/0000-0002-9494-0233

Werner Lehnert − *Institute of Energy and Climate Research, IEK-14: Electrochemical Process Engineering, Forschungszentrum Jülich GmbH, 52425 Jülich, Germany; Faculty of Mechanical Engineering, RWTH Aachen University, 52062 Aachen, Germany*

Complete contact information is available at: https://pubs.acs.org/10.1021/acsami.0c20690

Notes

The authors declare no competing financial interest.

■ ACKNOWLEDGMENTS

The authors acknowledge experimental support from Daniel Holtz and Stefanie Fischer. They would also like to thank Andreas Everwand for the SEM analysis and Lu Xia for the schematic illustration discussion. C.L. is also grateful for support from the China Scholarship Council (CSC).

■ NOMENCLATURE

C_{dl}, double-layer capacitance, F cm^{-2}
R_{DC}, DC resistance, Ω cm^2
R_K, kinetic resistance of OER, Ω cm^2
R_{hf}, high-frequency kinetic resistance, Ω cm^2
R_{lf}, low-frequency kinetic resistance, Ω cm^2
R_{ct}, charge-transfer resistance, Ω cm^2
R_w, Warburg resistance, Ω cm^2

■ GREEK SYMBOLS

τ, time constant

■ ABBREVIATIONS

CCM, catalyst-coated membrane
CPE, constant phase element
EDX, energy-dispersive X-ray spectroscopy
EIS, electrochemical impedance spectroscopy
FIB, focused ion beam
ICR, interfacial contact resistance
OER, oxygen evolution reaction
ORR, oxygen reduction reaction
PEM, polymer electrolyte membrane
PGM, platinum group metal
PTE, porous transport electrode
PTL, porous transport layer
SEM, scanning electron microscopy

■ REFERENCES

(1) Schultz, M. G.; Diehl, T.; Brasseur, G. P.; Zittel, W. Air pollution and climate-forcing impacts of a global hydrogen economy. *Science* **2003**, *302*, 624−627.
(2) Turner, J. A. Sustainable hydrogen production. *Science* **2004**, *305*, 972−974.
(3) Niether, C.; Faure, S.; Bordet, A.; Deseure, J.; Chatenet, M.; Carrey, J.; Chaudret, B.; Rouet, A. Improved water electrolysis using magnetic heating of FeC−Ni core−shell nanoparticles. *Nat. Energy* **2018**, *3*, 476−483.

(4) Mo, J.; Kang, Z.; Retterer, S. T.; Cullen, D. A.; Toops, T. J.; Green, J. B.; Mench, M. M.; Zhang, F.-Y. Discovery of true electrochemical reactions for ultrahigh catalyst mass activity in water splitting. *Sci. Adv.* **2016**, *2*, No. e1600690.
(5) Yu, L.; Zhu, Q.; Song, S.; McElhenny, B.; Wang, D.; Wu, C.; Qin, Z.; Bao, J.; Yu, Y.; Chen, S.; Ren, Z. Non-noble metal-nitride based electrocatalysts for high-performance alkaline seawater electrolysis. *Nat. Commun.* **2019**, *10*, 5106.
(6) Carmo, M.; Fritz, D. L.; Mergel, J.; Stolten, D. A comprehensive review on PEM water electrolysis. *Int. J. Hydrogen Energy* **2013**, *38*, 4901−4934.
(7) Ayers, K.; Danilovic, N.; Ouimet, R.; Carmo, M.; Pivovar, B.; Bornstein, M. Perspectives on Low-Temperature Electrolysis and Potential for Renewable Hydrogen at Scale. *Annu. Rev. Chem. Biomol. Eng.* **2019**, *10*, 219−239.
(8) Grigoriev, S. A.; Bessarabov, D. G.; Glukhov, A. S. On the contamination of membrane-electrode assembles of water electrolyzers with solid polymer electrolyte by the elements of titanium alloys. *Russ. J. Electrochem.* **2017**, *53*, 808−812.
(9) Liu, C.; Carmo, M.; Bender, G.; Everwand, A.; Lickert, T.; Young, J. L.; Smolinka, T.; Stolten, D.; Lehnert, W. Performance enhancement of PEM electrolyzers through iridium-coated titanium porous transport layers. *Electrochem. Commun.* **2018**, *97*, 96−99.
(10) Schuler, T.; De Bruycker, R.; Schmidt, T. J.; Büchi, F. N. Polymer Electrolyte Water Electrolysis: Correlating Porous Transport Layer Structural Properties and Performance: Part I. Tomographic Analysis of Morphology and Topology. *J. Electrochem. Soc.* **2019**, *166*, F270−F281.
(11) Stähler, M.; Stähler, A.; Scheepers, F.; Carmo, M.; Lehnert, W.; Stolten, D. Impact of porous transport layer compression on hydrogen permeation in PEM water electrolysis. *Int. J. Hydrogen Energy* **2020**, *45*, 4008−4014.
(12) Trinke, P.; Keeley, G. P.; Carmo, M.; Bensmann, B.; Hanke-Rauschenbach, R. Elucidating the Effect of Mass Transport Resistances on Hydrogen Crossover and Cell Performance in PEM Water Electrolyzers by Varying the Cathode Ionomer Content. *J. Electrochem. Soc.* **2019**, *166*, F465.
(13) Siracusano, S.; Baglio, V.; Di Blasi, A.; Briguglio, N.; Stassi, A.; Ornelas, R.; Trifoni, E.; Antonucci, V.; Aricò, A. S. Electrochemical characterization of single cell and short stack PEM electrolyzers based on a nanosized IrO2 anode electrocatalyst. *Int. J. Hydrogen Energy* **2010**, *35*, 5558−5568.
(14) Borgardt, E.; Giesenberg, L.; Reska, M.; Müller, M.; Wippermann, K.; Langemann, M.; Lehnert, W.; Stolten, D. Impact of clamping pressure and stress relaxation on the performance of different polymer electrolyte membrane water electrolysis cell designs. *Int. J. Hydrogen Energy* **2019**, *44*, 23556−23567.
(15) Arbabi, F.; Kalantarian, A.; Abouatallah, R.; Wang, R.; Wallace, J. S.; Bazylak, A. Feasibility study of using microfluidic platforms for visualizing bubble flows in electrolyzer gas diffusion layers. *J. Power Sources* **2014**, *258*, 142−149.
(16) Hackemüller, F. J.; Borgardt, E.; Panchenko, O.; Müller, M.; Bram, M. Manufacturing of Large-Scale Titanium-Based Porous Transport Layers for Polymer Electrolyte Membrane Electrolysis by Tape Casting. *Adv. Eng. Mater.* **2019**, *21*, 1801201.
(17) Borgardt, E.; Panchenko, O.; Hackemüller, F. J.; Giffin, J.; Bram, M.; Müller, M.; Lehnert, W.; Stolten, D. Mechanical characterization and durability of sintered porous transport layers for polymer electrolyte membrane electrolysis. *J. Power Sources* **2018**, *374*, 84−91.
(18) Grigoriev, S. A.; Millet, P.; Volobuev, S. A.; Fateev, V. N. Optimization of porous current collectors for PEM water electrolysers. *Int. J. Hydrogen Energy* **2009**, *34*, 4968−4973.
(19) Mo, J.; Steen, S.; Han, B.; Kang, Z.; Terekhov, A.; Zhang, F.-Y.; Retterer, S. T.; Cullen, D. A. Investigation of titanium felt transport parameters for energy storage and hydrogen/oxygen production. *13th International Energy Conversion Engineering Conference*, 2015; p 3914.
(20) Kang, Z.; Mo, J.; Yang, G.; Retterer, S. T.; Cullen, D. A.; Toops, T. J.; Green, J. B., Jr.; Mench, M. M.; Zhang, F.-Y. Investigation of thin/well-tunable liquid/gas diffusion layers exhibiting superior multifunctional performance in low-temperature electrolytic water splitting. *Energy Environ. Sci.* **2017**, *10*, 166−175.
(21) Ito, H.; Maeda, T.; Nakano, A.; Hwang, C. M.; Ishida, M.; Kato, A.; Yoshida, T. Experimental study on porous current collectors of PEM electrolyzers. *Int. J. Hydrogen Energy* **2012**, *37*, 7418−7428.
(22) Toops, T. J.; Brady, M. P.; Zhang, F.-Y.; Meyer, H. M.; Ayers, K.; Roemer, A.; Dalton, L. Evaluation of nitrided titanium separator plates for proton exchange membrane electrolyzer cells. *J. Power Sources* **2014**, *272*, 954−960.
(23) Feng, Q.; Yuan, X. Z.; Liu, G.; Wei, B.; Zhang, Z.; Li, H.; Wang, H. A review of proton exchange membrane water electrolysis on degradation mechanisms and mitigation strategies. *J. Power Sources* **2017**, *366*, 33−55.
(24) Bystron, T.; Vesely, M.; Paidar, M.; Papakonstantinou, G.; Sundmacher, K.; Bensmann, B.; Hanke-Rauschenbach, R.; Bouzek, K. Enhancing PEM water electrolysis efficiency by reducing the extent of Ti gas diffusion layer passivation. *J. Appl. Electrochem.* **2018**, *48*, 713−723.
(25) Rakousky, C.; Reimer, U.; Wippermann, K.; Carmo, M.; Lueke, W.; Stolten, D. An analysis of degradation phenomena in polymer electrolyte membrane water electrolysis. *J. Power Sources* **2016**, *326*, 120−128.
(26) Kang, Z.; Mo, J.; Yang, G.; Li, Y.; Talley, D. A.; Retterer, S. T.; Cullen, D. A.; Toops, T. J.; Brady, M. P.; Bender, G.; Pivovar, B. S.; Green, J. B.; Zhang, F.-Y. Thin film surface modifications of thin/tunable liquid/gas diffusion layers for high-efficiency proton exchange membrane electrolyzer cells. *Appl. Energy* **2017**, *206*, 983−990.
(27) Rakousky, C.; Keeley, G. P.; Wippermann, K.; Carmo, M.; Stolten, D. The stability challenge on the pathway to high-current-density polymer electrolyte membrane water electrolyzers. *Electrochim. Acta* **2018**, *278*, 324−331.
(28) Millet, P.; Grigoriev, S. Water electrolysis technologies. *Renewable Hydrogen Technologies: Production, Purification, Storage, Applications and Safety*; Newnes, 2013; pp 19−41.
(29) Liu, C.; Shviro, M.; Gago, A. S.; Zaccarine, S. F.; Bender, G.; Gazdzicki, P.; Morawietz, T.; Biswas, I.; Rasinski, M.; Everwand, A.; Schierholz, R.; Pfeilsticker, J.; Müller, M.; Lopes, P. P.; Eichel, R. A.; Pivovar, B.; Pylypenko, S.; Friedrich, K. A.; Lehnert, W.; Carmo, M. Exploring the Interface of Skin-Layered Titanium Fibers for Electrochemical Water Splitting. *Adv. Energy Mater.* **2021**, *11*, 2002926.
(30) Kang, Z.; Yang, G.; Mo, J.; Li, Y.; Yu, S.; Cullen, D. A.; Retterer, S. T.; Toops, T. J.; Bender, G.; Pivovar, B. S.; Green, J. B.; Zhang, F.-Y. Novel thin/tunable gas diffusion electrodes with ultra-low catalyst loading for hydrogen evolution reactions in proton exchange membrane electrolyzer cells. *Nano Energy* **2018**, *47*, 434−441.
(31) Choe, S.; Lee, B.-S.; Cho, M. K.; Kim, H.-J.; Henkensmeier, D.; Yoo, S. J.; Kim, J. Y.; Lee, S. Y.; Park, H. S.; Jang, J. H. Electrodeposited IrO2/Ti electrodes as durable and cost-effective anodes in high-temperature polymer-membrane-electrolyte water electrolyzers. *Appl. Catal., B* **2018**, *226*, 289−294.
(32) Liu, S.; Rasinski, M.; Rahim, Y.; Zhang, S.; Wippermann, K.; Reimer, U.; Lehnert, W. Influence of operating conditions on the degradation mechanism in high-temperature polymer electrolyte fuel cells. *J. Power Sources* **2019**, *439*, 227090.
(33) Bender, G.; Carmo, M.; Smolinka, T.; Gago, A.; Danilovic, N.; Mueller, M.; Ganci, F.; Fallisch, A.; Lettenmeier, P.; Friedrich, K. A.; Ayers, K.; Pivovar, B.; Mergel, J.; Stolten, D. Initial approaches in benchmarking and round robin testing for proton exchange membrane water electrolyzers. *Int. J. Hydrogen Energy* **2019**, *44*, 9174−9187.
(34) Brug, G. J.; Van Den Eeden, A. L. G.; Sluyters-Rehbach, M.; Sluyters, J. H. The analysis of electrode impedances complicated by the presence of a constant phase element. *J. Electroanal. Chem.* **1984**, *176*, 275−295.
(35) Hirschorn, B.; Orazem, M. E.; Tribollet, B.; Vivier, V.; Frateur, I.; Musiani, M. Determination of effective capacitance and film

https://doi.org/10.1021/acsami.0c20690
ACS Appl. Mater. Interfaces 2021, 13, 16182−16196

thickness from constant-phase-element parameters. *Electrochim. Acta* **2010**, *55*, 6218−6227.
(36) Conway, B. E.; Liu, T. C. Characterization of electrocatalysis in the oxygen evolution reaction at platinum by evaluation of behavior of surface intermediate states at the oxide film. *Langmuir* **1990**, *6*, 268−276.
(37) Zhao, S.; Yu, H.; Maric, R.; Danilovic, N.; Capuano, C. B.; Ayers, K. E.; Mustain, W. E. Calculating the electrochemically active surface area of iridium oxide in operating proton exchange membrane electrolyzers. *J. Electrochem. Soc.* **2015**, *162*, F1292.
(38) Slavcheva, E.; Radev, I.; Bliznakov, S.; Topalov, G.; Andreev, P.; Budevski, E. Sputtered iridium oxide films as electrocatalysts for water splitting via PEM electrolysis. *Electrochim. Acta* **2007**, *52*, 3889−3894.
(39) Marshall, A.; Børresen, B.; Hagen, G.; Tsypkin, M.; Tunold, R. Electrochemical characterisation of $Ir_xSn_{1-x}O_2$ powders as oxygen evolution electrocatalysts. *Electrochim. Acta* **2006**, *51*, 3161−3167.
(40) Bernt, M.; Siebel, A.; Gasteiger, H. A. Analysis of voltage losses in PEM water electrolyzers with low platinum group metal loadings. *J. Electrochem. Soc.* **2018**, *165*, F305.
(41) Xu, W.; Scott, K. The effects of ionomer content on PEM water electrolyser membrane electrode assembly performance. *Int. J. Hydrogen Energy* **2010**, *35*, 12029−12037.
(42) Slavcheva, E.; Ganske, G.; Topalov, G.; Mokwa, W.; Schnakenberg, U. Effect of sputtering parameters on surface morphology and catalytic efficiency of thin platinum films. *Appl. Surf. Sci.* **2009**, *255*, 6479−6486.
(43) Hellström, M.; Quaranta, V.; Behler, J. One-dimensional vs. two-dimensional proton transport processes at solid−liquid zinc-oxide−water interfaces. *Chem. Sci.* **2019**, *10*, 1232−1243.

https://doi.org/10.1021/acsami.0c20690
ACS Appl. Mater. Interfaces 2021, 13, 16182−16196